Hardware Implementation of COTS Avionics System on Unmanned Aerial Vehicle Platforms

Yoo-Hsiu Yeh
Carnegie Mellon University Silicon Valley, Moffett Field, CA, 94035

Parth Kumar
Polytechnic Institute of New York University, Brooklyn, NY 11201

Abraham Ishihara, Ritchie Lee
Carnegie Mellon University Silicon Valley, Moffett Field, CA, 94035

Corey Ippolito
NASA Ames Research Center, Moffett Field, CA, 94035

This paper describes the latest work on the NASA Exploration Aerial Vehicle (EAV) and Experimental Sensor-Controlled Aerial Vehicle (XSCAV). The EAV and XSCAV are Unmanned Aerial Vehicles developed in support of control systems research. The paper details requirements and design of new avionics hardware. Techniques used for identification of the EAV system parameters using corrected flight data are also described. The identified system parameters are used to implement a simulation of the EAV, in both Matlab and Reflection, for verification.

I. Introduction

THE NASA Exploration Aerial Vehicle (EAV) Lab operates two instrumented Commercial-Off-The-Shelf (COTS) aerial platforms for testing novel control systems. The main aircraft is the EAV, a quarter-scale Cessna 182 that serves as the primary test platform for control systems. It is low-cost and easy to maintain and has already been certified by the FAA. Previous research carried out with the EAV has included testing of the NASA Ames Intelligent Flight Controller (IFC) [1], Polymorphic Control Systems (PCS) [2], and simulation work with the Trajectory Linearization Controller (TLC) [15] in conjunction with Payload Directed Flight (PDF) project [3]. The EAV will be used to support preliminary low-risk testing of adaptive controllers developed under the NASA Ames Integrated Resilient Aircraft Control (IRAC) project.

Although the EAV has proven itself to be a capable workhorse for the testing of control system designs, it has limited payload capabilities. Thus, a second, larger platform was acquired, the Experimental Sensor-Controlled Aerial Vehicle (XSCAV). The XSCAV is a 50% scale J3 Piper Cub with payload capacity of over fifty pounds [3].

Both EAV and XSCAV are outfitted with the same avionics and control systems, allowing for parallel development. The avionics hardware is continually upgraded to provide state-of-the-art processing power and sensors needed to carry out respective tests.

Figure 1. NASA EAV (left) and NASA XSCAV (right).

The remainder of this paper is organized as follows: discussion of the design and testing process for the new EAV/XSCAV avionics hardware, analysis of corrected flight data logged on the EAV for System Identification, and finally, simulation results.

II. EAV Airframe Modifications

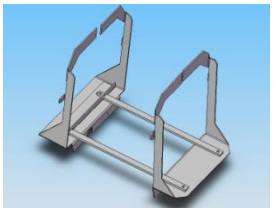

Several modifications and improvements have been made to the EAV in support of future research since the last update in [1], most namely the addition of an aluminum rib support structure and the design of a custom avionics box. These changes affect the weight and balance of the plane. Initial flight tests with the modifications will include system identification maneuvers to check for changes in the airplane model.

Previous papers [1] have documented the effects of stress on the EAV airframe. The added weight (about 5 pounds) of the avionics box reduces the maneuverability of the aircraft. High-g maneuvers have previously resulted in snapping of the wing struts and failure of the fuselage strut mounts. These issues were addressed by replacing the factory struts with stronger custom-built struts, and strengthening the mounting points on the fuselage and wings.

The new avionics and avionics box will add about a pound to the final weight. To address the problem of the additional weight, as well as a possibility of future high-g maneuvers, a custom set of aluminum ribs was designed, which are shown in Figure 2.

Figure 2. EAV Rib structure.

The ribs distribute the stress between the six areas of the EAV airframe with the heaviest load: the wing bar area, from which most the lift of the wings is distributed to the fuselage, the body wing strut mounts, which also distribute some of the stress from the lift, and the landing gear, which pass the impact of hard landings into the belly of the plane.

III. Avionics Design

The capability to run real-time processing of potentially large amounts of sensor data adds versatility to the avionics system, but also loads the flight computer. For example, if run on the same processor as the control system, vision processing the body camera images as described in [4] to generate a real-time trajectory, could interfere with the main autopilot control loops. To resolve these issues, a second, faster CPU was introduced to the avionics stack. To supply the larger combined power draw of the two CPUs, the former power supply was replaced with a higher wattage DC/DC power supply. A more in-depth discussion of the former EAV avionics box and components can be found in [1].

A. Overview of Existing UAV Avionics Designs

A quick comparison of best practices among Unmanned Aerial Vehicle (UAV) groups reveals many similarities, many of which are also in place on the EAV. A brief overview of existing fixed-wing UAV avionics designs in the literature is compiled here.

A number of groups opt for avionics in the PC/104 form factor, including the Stanford Dragonfly, NASA FASER, and NASA AirSTAR, for their test plane [11][12][13]. Georgia Tech opted to design a custom avionics board [6], while the group at the University of Colorado, Boulder, has designed their own modular units called Naiads [14]. Other groups opt for commercial autopilots such as the Piccolo or Micropilot.

Additional comparisons will be added here, including comparisons of custom avionics and prepackaged kits.

B. Design of Custom Avionics Box

As mentioned earlier, the addition of a second CPU increased the height of the avionics stack. In order to compensate for the increased height of the stack inside the EAV payload bay, the stack was placed horizontally. To prevent the need for further redesigns for future board additions, a custom avionics box was designed around an extended PC/104 stack. The main requirements for the avionics box are listed in the table below.

Table 1. Avionics Box Design Requirements.

Area	Requirement
Electrical	Must shield components from outside radiation and keep inside radiation from affecting pilot control receiver. Holes and edges should be kept to a minimum.
Mechanical	Must hold standard PC/104 boards, allowing extra space for standard connectors off the sides.

Mechanical	Must provide sufficient cooling for operation of internal components.
Mechanical	Must be self-contained, easy to swap in and out.
Mechanical	Must provide vibration isolation to avionics components.
Mechanical	Must be as lightweight as possible, at or under 5 pounds.
Mechanical	Must fit within EAV payload bay.

Electrical: The final box design is bent from 0.040" aluminum, anodized for insulation. The bottom is a single U-shaped piece. The two sides slide out without affecting any other components, allowing connectors on the top to remain attached during ground testing, as can be seen in the left image in Figure 3. All edges are overhung to attenuate EMI, and at least two attachment screws are used per edge to keep gaps under six centimeters apart, which provides a continuous shield against frequencies under 5GHz. Flat tapped screws were used to secure attachment points, and anodization on the box around attachment points was removed to ensure solid electrical connection. Guidelines for shielded enclosure design were based on [7] and [8].

[Diagram of FFT of noise outside the box with sides with and without holes.]

Mechanical: The box holds up to thirteen PC/104 boards and has multiple pre-drilled holes and passthroughs. For mounting into the EAV, the box directly bolts to twin rails that slide into the ribs described in the previous section. Vibration isolation is handled inside of the box, where the PC/104 stack is held to the box by eight Parvus Bumper Beans. The front of the box is directly adjacent to the EAV gas tank, so battery connectors are on the rear panel. The center of the rear panel can be swapped out for different connectors as needed. Inside the box behind the points of attachment, type FE self-clinching PEM® miniature fasteners were pressed into the metal instead of nuts to reduce weight and remove the need to reach inside the box.

Five rows of small ventilation holes were drilled along the front end of either side panel. Two +12V CPU fans on the back pull air from the front into the box, drawing heat away from the box components. The HSPC104-SER is a switching power supply with up to 95% efficiency, so while it may add heat to the box, the main source of heat will be the ADL945PC CPU, drawing an average of two to three amps. The CPU is rated for temperatures up to 60˚C, or 140˚F.

The slot on the top of the box was left for ease of swapping out the data log compact flash cards, without having to disassemble the box after every flight test. Once assembled, the box and stack is a self-contained unit.

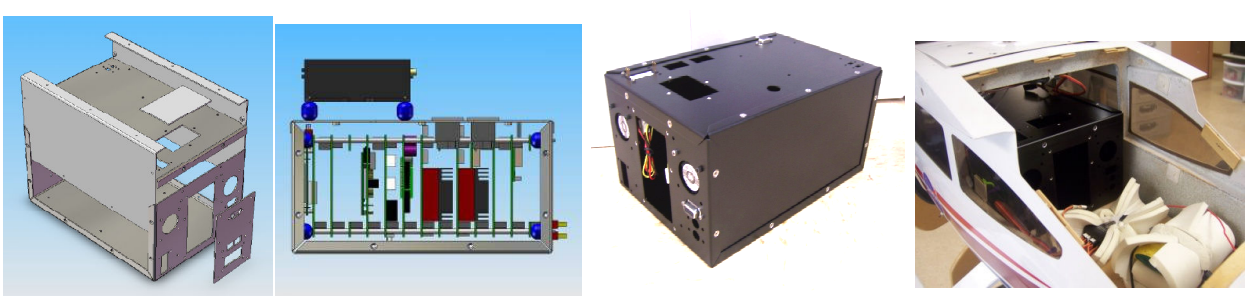

Figure 3. Final Avionics Box Design in Solidworks (left, middle) and Actual (right).

Table 2. Final Avionics Box Specifications.

Box Specifications	
Length	9.44 in. (23.98 cm)
Width	6.30 in. (16.00 cm)
Height	4.78 in. (12.14 cm)

C. Redesign of Avionics System

The main avionics for the EAV/XSCAV were chosen in the PC/104 form factor for its small size, ruggedness, and processor capability. Remaining avionics were chosen with keeping compatibility with the PC/104 form factor in mind. The HBC101 servo controller and the compact flash card readers were mounted on adapter plates to fit in the PC/104 stack. A custom PC/104-sized PCB mount was designed to mount and electrically interface the avionics with the MHX-910 radio modem. This board provides power and a RS232-to-TTL converter for the modem unit. The main requirements for the avionics system are listed in the table below.

Table 3. Avionics System Requirements.

Area	Requirement
Electrical	Noise carried between boards by cables must be kept to a minimum.
Electrical	Avionics must be grounded to the box as close to the batteries as possible.
Electrical	All wires must be rated to carry their maximum projected current.
Electrical	Servo Passthrough board must withstand Stall of two servos (5A).
Electrical	Avionics components must operate properly in typical operating EMI environment.
Mechanical	Avionics components must be rated to withstand vibration environment.
Mechanical	All fasteners and cables must have some kind of secondary securing mechanism for vibration.
Mechanical	Cables must be bundled to minimize strain and contact with other components.
Mechanical	Heat sinks/fans/inlets must remain unobstructed in the final configuration.
Mechanical	Avionics components must be rated to withstand temperature environment.

Table 4. Avionics System Components

Component	Manufacturer	Model	Description
Power Supply	Tri-M Systems	HPSC104-SER	168W DC/DC High Power Vehicle Power Supply
Servo Controller	Pontech	HBC101	A/D and hybrid motor controller board
Hard Drive (ground test only)	Western Digital	Scorpio	160GB EIDE Notebook Hard Drive
CF Cards	Sandisk	Extreme III CF, 8GB	Two (2x) 8GB CF cards
CPU	Advanced Digital Logic	ADL945PC-L2400	DualCore 1.66GHz, 2M cache PC/104
RTOS CPU	Digital Logic	MSMP3SEV	SmartCore P3-700, 700MHz, 256MB
CPU I/O	Parvus	COM-1274	PC/104 8-Port Serial Module with CAN 2.0
INS/GPS	Athena Controls, Inc.	Guidestar GS111m	Digital IMU/INS/GPS Sensor Suite
Radio Modem	Microhard System, Inc.	MHX-910	ISM Band 900Mhz RF Radio Modem
Fan	(Unknown)	(Unknown)	Cooling Fan
2.4Ghz Video System	(Unknown)	(Unknown)	Video camera and transmitter

Electrical: As shown in the Figure 4, the avionics were arranged in the box to minimize cable length, place the heaviest components closer to the EAV center of gravity, and allow for greater heat dissipation. For each of the custom cables, the wire gauge was chosen based on temperature rise given maximum current load. All cables were twisted or shielded, if possible, to reduce noise interference within box. Shielded cables were grounded on one side only, as described in [--]. Battery Ground was tied to Chassis ground at one location near the entrance of the power cables to avoid ground loops.

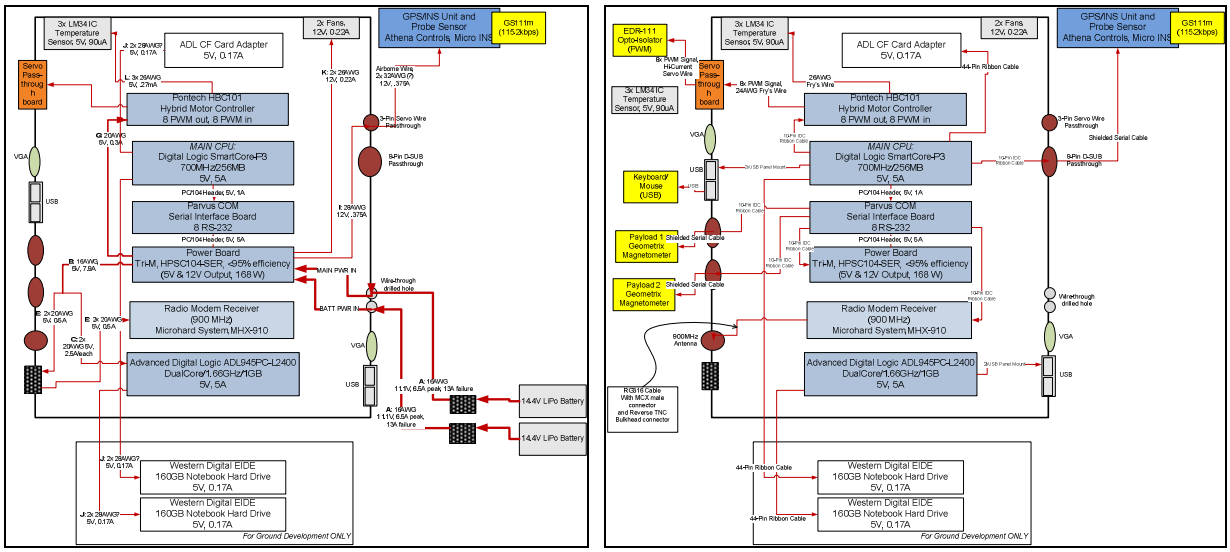

Figure 4. Power (left) and Communications (right) Wiring for Avionics Box.

The avionics are powered by two 3S2P LiPo batteries in parallel, providing 11.1V nominal voltage with 10000mAh combined rated capacity. Power draw calculations were also carried out to gauge expected operating time and ensure that power systems could supply the current necessary.

Mechanical: All custom connectors have secondary latching mechanisms. If existing connectors did not have secondary latching, a layer of RTV silicone rubber was applied to both sides of the connection to serve as secondary reinforcement. RTV was also over applied over screw terminal connectors to the possibility of loose screws due to vibration.

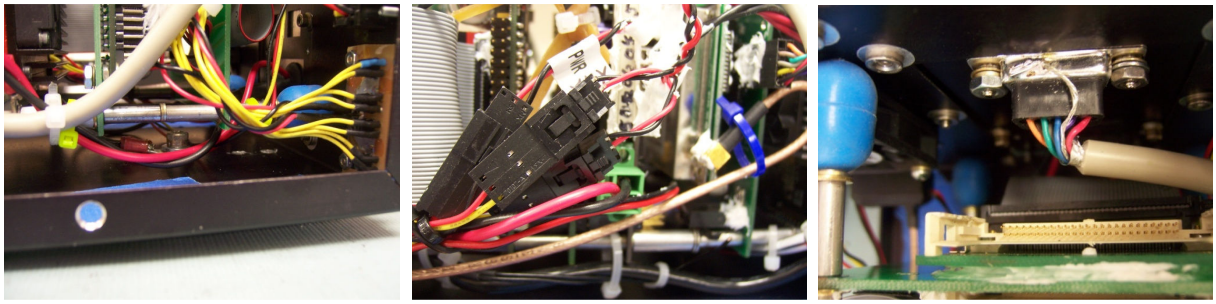

Figure 5. Grounding avionics to chassis (left), secondary latching mechanisms (center), and grounded shielded cable (right).

D. Redesign of Actuator System

The actuator system was re-designed to provide redundancy in case of loss of signal, loss of power, and battery short-circuits. The servos are divided into two banks, either of which can be used for partial control of the plane. A Redundancy Failure Scenario graph is shown in Figure 9.

The avionics system ties into the actuator system through an optical isolation unit, and is considered a secondary control source. In the event of any avionics box issues, control will be taken back by the primary pilot over RC control. This process is described more in detail in [1], with the exception being that the Safety Switch has been replaced by two 4-channel multiplexers.

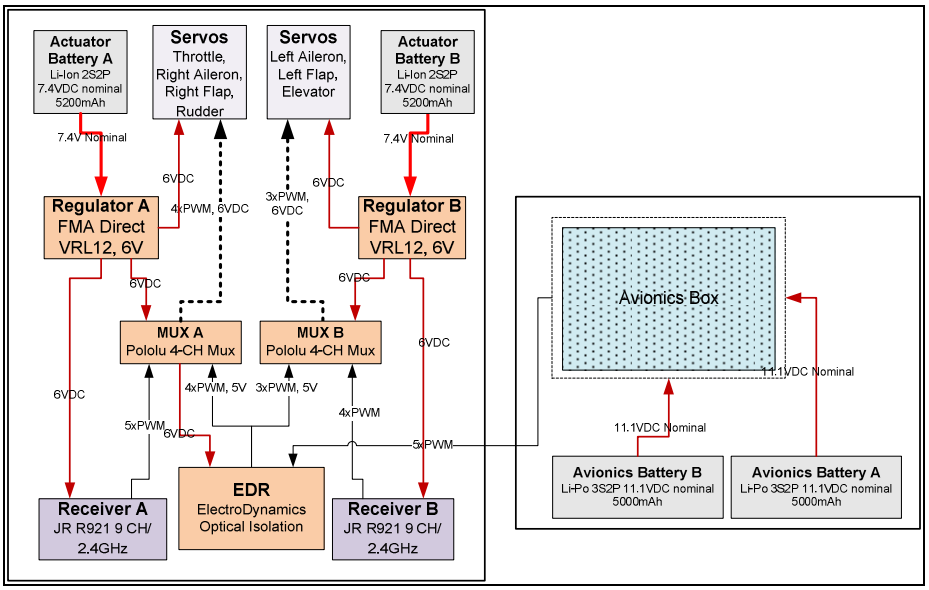

Figure 6. Actuator Design and Interface with Avionics.

[Figure 9. Failure Scenario Redundancy Graph.]

IV. EAV System Identification

System identification has been carried out on EAV flight test data by members of the EAV lab, and the results have been published in [1] and [2]. However, a slight error in the rotation matrix used to calculate the p, q, and r data values for the system identification in [1] was discovered, so a new corrected system identification was run. The error is shown below.

Equation 1. PQR Transformation with (left) and without (right) Heading/Yaw error.

$$\begin{bmatrix} q \\ p \\ -r \end{bmatrix} = \begin{bmatrix} p_{sl} \\ q_{sl} \\ r_{sl} \end{bmatrix} = \begin{bmatrix} 1 & 0 & -\sin(\theta) \\ 0 & \cos(\phi) & \sin(\phi)\cos(\theta) \\ 0 & -\sin(\phi) & \sin(\phi)\cos(\theta) \end{bmatrix} \begin{bmatrix} \dot{\phi} \\ \dot{\theta} \\ \dot{\psi} \end{bmatrix} \qquad \begin{bmatrix} q_{err} \\ p_{err} \\ -r_{err} \end{bmatrix} = \begin{bmatrix} 1 & 0 & -\sin(\theta) \\ 0 & \cos(\phi) & \sin(\phi)\cos(\theta) \\ 0 & -\sin(\phi) & \sin(\phi)\cos(\theta) \end{bmatrix} \begin{bmatrix} \dot{\phi} \\ \dot{\theta} \\ -\dot{\psi} \end{bmatrix}$$

Before April 2010, there will be an additional system identification flight of the EAV with the new modifications for additional adjustments to this model. These system identification procedures can be readily applied to new flight data.

A. Aircraft Dynamical Model

The aerodynamic moment model was based on formulas from [5] and [6], with a few minor modifications.

Longitudinal:

$$\dot{q} = \frac{\bar{q}S\bar{c}}{J_y}\left(C_{m0} + C_{m\alpha}\alpha + C_{m\delta e}\delta_e + \frac{\bar{c}}{2V_T}C_{mq}q\right) - \frac{I_p}{I_y}\omega_p r - \frac{(J_x - J_z)}{J_y}pr - \frac{J_{xz}}{J_y}(p^2 - r^2)$$

Lateral:

$$\dot{p} - \dot{r}\frac{I_{xz}}{I_x} = \frac{\bar{q}Sb}{I_x}\left(C_{l0} + C_{l\beta}\beta + C_{l\delta a}\delta_a + C_{l\delta r}\delta_r + \frac{b}{2V_T}\left(C_{lp}p + C_{lr}r\right)\right) + \frac{I_{xz}}{I_x}(pq) - \frac{(I_z - I_y)}{I_x}qr - \frac{I_p}{I_x}\omega_p q$$

$$r - \dot{p}\frac{I_{xz}}{I_z} = \frac{\bar{q}Sb}{I_z}\left(C_{n0} + C_{n\beta}\beta + C_{n\delta a}\delta_a + C_{n\delta r}\delta_r + \frac{b}{2V_T}\left(C_{np}p + C_{nr}r\right)\right) - \frac{I_{xz}}{I_z}(qr) - \frac{(I_y - I_x)}{I_z}pq - \frac{I_p}{I_z}\omega_p q$$

The least mean squares optimization problem is solved as follows:

$$\hat{\theta} = (X^T X)^{-1} X z \ ,$$

where we assign $z = \dot{p}, \dot{q}$ and $\dot{r}$ for each set of coefficients C_l, C_m, and C_n, respectively. We can rewrite the moment equations as:

$$\dot{p} = \sum_{i=1}^{N_l} h_{l_i} w_{l_i}^*$$

$$\dot{q} = \sum_{i=1}^{N_m} h_{m_i} w_{m_i}^*$$

$$\dot{r} = \sum_{i=1}^{N_n} h_{n_i} w_{n_i}^*$$

where:

Table 5. Setting up the Least Squares problem.

Lateral, C_l:	**Longitudinal, C_m:**	**Lateral, C_n:**
Abbreviated Linear Version (no cross terms)		
$h_{l1} = 1 \quad w_{l1}^* = \bar{q}Sb(c_3 C_{l0} + c_4 C_{n0})$ $h_{l2} = p \quad w_{l2}^* = \bar{q}Sb\frac{b}{2V_T}(c_3 C_{lp} + c_4 C_{np})$ $h_{l3} = r \quad w_{l3}^* = \bar{q}Sb\frac{b}{2V_T}(c_3 C_{lr} + c_4 C_{nr})$ $h_{l4} = \beta \quad w_{l5}^* = \bar{q}Sb(c_3 C_{l\beta} + c_4 C_{n\beta})$ $h_{l5} = \delta_a \quad w_{l5}^* = \bar{q}Sb(c_3 C_{l\delta a} + c_4 C_{n\delta a})$ $h_{l6} = \delta_r \quad w_{l6}^* = \bar{q}Sb(c_3 C_{l\delta r} + c_4 C_{n\delta r})$	$h_{m1} = 1 \quad w_{m1}^* = \bar{q}S\bar{c}c_7 C_{m0}$ $h_{m2} = q \quad w_{m5}^* = \bar{q}S\bar{c}c_7 \frac{\bar{c}}{2V_T} C_{mq}$ $h_{m3} = \alpha \quad w_{m2}^* = \bar{q}S\bar{c}c_7 C_{m\alpha}$ $h_{m4} = \delta_e \quad w_{m3}^* = \bar{q}S\bar{c}c_7 C_{m\delta e}$ $h_{m5} = r \quad w_{m4}^* = \frac{I_p}{I_y}\omega_p$	$h_{n1} = 1 \quad w_{n1}^* = \bar{q}Sb(c_4 C_{l0} + c_9 C_{n0})$ $h_{n2} = p \quad w_{n2}^* = \bar{q}Sb\frac{b}{2V_T}(c_4 C_{lp} + c_9 C_{np})$ $h_{n3} = r \quad w_{n3}^* = \bar{q}Sb\frac{b}{2V_T}(c_4 C_{lr} + c_9 C_{nr})$ $h_{n4} = \beta \quad w_{n4}^* = \bar{q}Sb(c_4 C_{l\beta} + c_9 C_{n\beta})$ $h_{n5} = \delta_a \quad w_{n5}^* = \bar{q}Sb(c_4 C_{l\delta a} + c_9 C_{n\delta a})$ $h_{n6} = \delta_r \quad w_{n6}^* = \bar{q}Sb(c_4 C_{l\delta r} + c_9 C_{n\delta r})$
Full Nonlinear Version Additions (cross terms)		
$h_{l7} = q \quad w_{l7}^* = -\frac{I_p}{I_z}\omega_p$ $h_{l8} = rq \quad w_{l8}^* = -\frac{(I_z - I_y)}{I_x}$ $h_{l9} = pq \quad w_{l9}^* = \frac{I_{xz}}{I_x}$	$h_{m6} = pr \quad w_{m6}^* = -\frac{(I_x - I_z)}{I_y}$ $h_{m7} = p^2 - r^2 \quad w_{m7}^* = -\frac{I_{xz}}{I_y}$ $h_{m8} = \dot{\alpha} \quad w_{m8}^* = \bar{q}S\bar{c}c_7 \frac{\bar{c}}{2V_T} C_{m\dot{\alpha}}$	$h_{n7} = q \quad w_{n7}^* = -\frac{I_p}{I_z}\omega_p$ $h_{n8} = rq \quad w_{n8}^* = \frac{I_{xz}}{I_z}$ $h_{n9} = pq \quad w_{n9}^* = -\frac{(I_y - I_x)}{I_z}$

Table 6. EAV Properties.

Properties	**Values [units]**
Aerodynamic Reference area (S)	0.804 [m^2]
Longitudinal reference length ($\bar{c}$)	1.9495 [m]
Lateral reference length (b)	2.406 [m]
Free stream airspeed (V_0)	mean (V_{air}) [m/s]
Inertias I_x, I_y, I_z	4.74, 7.73, 9.8 [kg-m^2] *
Inertia I_{xz}	2.48 [kg-m^2] *

* Modified from Roskam full-scale Cessna data

B. System Identification Results

The least squares procedure was run on multiple flight datasets to obtain estimates of $\boldsymbol{C_l}$, $\boldsymbol{C_m}$, and $\boldsymbol{C_n}$. For each data set, we computed two different scores. The first was measured by a normalized MSE applied to the dataset. The second was a generalization score, in which the MSE was calculated based on how a model performed on untrained data sets. A weighted average of the two scores was then used to determine the optimal set of coefficients. The final $\boldsymbol{C_l}$, $\boldsymbol{C_m}$, and $\boldsymbol{C_n}$ coefficients and plots of the models with the best score are shown below.

Table 7. Calculated Coefficients.

C_{l0} 3.6679e-05	C_{lp} -0.0179	C_{lr} -0.0382	$C_{l\beta}$ 1.177e-03	$C_{l\delta_{ail}}$ -7.666e-03	$C_{l\delta_{rud}}$ -4.357e-03
	C_{m0} -2.5063e-03	C_{mq} -0.2769	$C_{m\alpha}$ -0.3946	$C_{m\delta_{ele}}$ -0.5604	
C_{n0} 1.0482e-05	C_{np} -0.0179	C_{nr} -3.716e-03	$C_{n\beta}$ 7.2972e-04	$C_{n\delta_{ail}}$ -2.5132e-03	$C_{n\delta_{rud}}$ -6.5092e-04

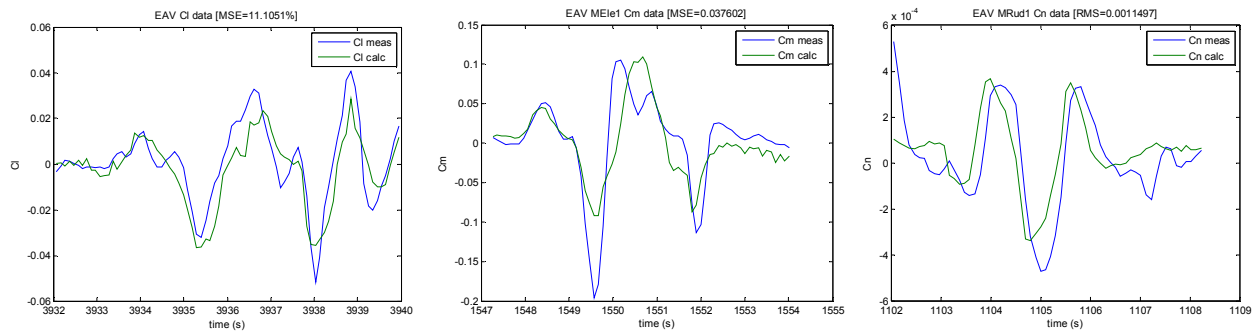

Figure 7. Comparisons of measured and estimated Cl, Cm, and Cn values.

V. Matlab Simulation

Upcoming flight tests of the EAV will most likely involve controller designed by the NASA Ames Integrated Resilient Aircraft Control (IRAC) project. One of the IRAC project's main controllers is the Model Reference Adaptive Control (MRAC), as developed in detail in [9]. For controller design, we assume a linear inner-loop model given by:

$$\dot{\omega} = F_1\omega + F_2\sigma + G\delta$$

where

$$\omega = \begin{bmatrix} p \\ q \\ r \end{bmatrix} \qquad F_1 = \begin{bmatrix} w_{l_2}^* & w_{l_7}^* & w_{l_3}^* \\ 0 & w_{m_2}^* & w_{m_5}^* \\ w_{n_2}^* & w_{n_7}^* & w_{n_3}^* \end{bmatrix}$$

$$\sigma = \begin{bmatrix} 1 \\ \alpha \\ \beta \end{bmatrix} \qquad F_2 = \begin{bmatrix} w_{l_1}^* & 0 & w_{l_4}^* \\ w_{m_1}^* & w_{m_3}^* & 0 \\ w_{n_1}^* & 0 & w_{n_4}^* \end{bmatrix}$$

$$\delta = \begin{bmatrix} \delta_a \\ \delta_e \\ \delta_r \end{bmatrix} \qquad G = \begin{bmatrix} w_{l_5}^* & 0 & w_{l_6}^* \\ 0 & w_{m_4}^* & 0 \\ w_{n_5}^* & 0 & w_{n_6}^* \end{bmatrix}$$

Using our offline system identification results this becomes:

$$F_1 = \begin{bmatrix} -2.5093 & -0.0580 & -5.2579 \\ 0 & -0.5839 & 2.7239 \\ 1.0155 & 0.0585 & 1.7834 \end{bmatrix}$$

$$F_2 = \begin{bmatrix} 0.0825 & 0 & -2.1044 \\ -0.0964 & -15.1835 & 0 \\ 0.0066 & 0 & 2.3619 \end{bmatrix}$$

$$G = \begin{bmatrix} -16.8037 & 0 & -10.6250 \\ 0 & -21.5610 & 0 \\ -3.1348 & 0 & 2.4701 \end{bmatrix}$$

This state space description is convenient for MRAC controller analysis. Results from the simulation are shown in Fig.10.

VI. Reflection Simulation

After testing in Matlab, the model will be ported over to the NASA Reflection software architecture. The Reflection architecture is a real-time component-based plug-and-play architecture described in detail in [10], especially in regards to its use on the EAV. The architecture is the main software running on the avionics processors.

Running the model in Reflection provides a variety of benefits:

1. Visualization of the aircraft
2. Ability to fly the simulation via pilot joystick input
3. Ease in moving software from simulation testing to hardware-in-the-loop testing, and finally flight testing

Results from the Reflection Simulation will be documented after testing.

MRAC simulation based on the system identification results is shown in Fig. 11.

VII. Conclusions

This paper reviews the design and testing process for the new EAV/XSCAV avionics hardware. Additionally, we have presented several models obtained via offline system identification, as well as MRAC control simulation based on these models. New system identification flights EAV were carried out under the new configurations, and the results were compared to the previous results. These improvements in hardware and aircraft model will help the EAV continue to serve as the main platform for preliminary low-risk testing of adaptive controllers developed under the NASA Ames Integrated Resilient Aircraft Control (IRAC) project and others.

References:

[1]C. Ippolito, YH Yeh, and J. Kaneshige. *Neural Adaptive Flight Control Testing on an Unmanned Experimental Aerial Vehicle* . AIAA-2008-2827. May 2007.

[2]C. Ippolito, S. Joo, K. Al-Ali, and YH Yeh. *Polymorphic Control Reconfiguration in an Autonomous UAV with UGV Collaboration.* Aerospace Conference, 2008 IEEE. March 2008.

[3]C. Ippolito, S. Campbell, and YH Yeh. *A Trajectory Generation Approach for Payload Directed Flight.* AIAA-2009-1351. January 2009.

[4]Ritchie Lee and Corey Ippolito. *A Perception and Mapping Approach for Plume Detection in Payload Directed Flight.* AIAA-2009-1898. April 2009.

[5]V. Klein and E.A. Morelli. *Aircraft System Identification: Theory and Practice*. AIAA, AIAA Education Series. 2006.

[6]Dongwon Jung. *Hierarchical Path Planning and Control of a Small Fixed-Wing UAV: Theory and Experimental Validation.* Thesis Presented to Georgia Institute of Technology. December 2007.

[7]F.B. Beck, C.R. Cockrell, and M.D. Deshpande. *Electromagnetic Shielding Effectiveness of Rectanguular Enclosure with Perforated Walls*. Proceedings of the 18th Digital Avionics Conference. October 1999.

[8]Morrison, Ralph. *Grounding and Shielding: Circuits and Interference.* Wiley-IEEE Press, 5th edition. March 16, 2007.

[9]Nhan Nguyen and Kalmanje Krishnakumar. *Hybrid Intelligent Flight Control with Adaptive Learning Parameter Estimation*. AIAA 2007-2841. May 2007.

[10]C. Ippolito, G. Pisanich, and K. Al-Ali. *Component-Based Plug-and-Play Methodologies for Embedded Technology Development*. AIAA-2005-7122. September 2005.

[11]Thomas Jordan and Roger Bailey. *NASA Langley's AirSTAR Testbed – A Subscale Flight Test Capability for Flight Dynamics and Control System Experiments*. AIAA-2008-6660. August 2008.

[12]D.B. Owens, D.E. Cox, and E.A. Morelli. *Development of a Low-Cost Sub-Scale Aircraft for Flight Research: The FASER Project.* AIAA-2006-3306. June 2006.

[13]Jung Soon Jang and Claire J. Tomlin. *Design and Implementation of a Low Cost, Hierarchical and Modular Avionics Architecture for the DragonFly UAVs.* AIAA-2002-4465. August 2002.

[14]J. Elston, B. Agrow, and E. Frew. *A Distributed Avionics Package for Small UAVs.* AIAA 2005-6984. September 2005.

[15]T. Adami, J. Zhu, et. all. *Six DoF Trajectory Tracking for Payload Directed Flight Using Trajectory Linearization Control*. AIAA-2009-1897. April 2009.